This article has been accepted for publication in IEEE Access. This is the author's version which has not been fully edited and content may change prior to final publication. Citation information: DOI 10.1109/ACCESS.2022.3199732

IEEE Access
Multidisciplinary | Rapid Review | Open Access Journal

Date of publication xxxx 00, 0000, date of current version xxxx 00, 0000.

Digital Object Identifier 10.1109/ACCESS.2017.Doi Number

Modeling, Analysis and Proportional Resonant and Proportional Integral based Control Strategy for Single Phase Quasi- Z Source Inverters

Seyfettin Vadi[1], (Student Member IEEE), Ramazan Bayindir[2], (Senior Member IEEE)

[1]Department of Electronics and Automation, Vocational School of Technical Sciences, Gazi University, 6170 Ankara, Turkey.
[2]Department of Electrical and Electronics Engineering, Faculty of Technology, Gazi University, 6170 Ankara, Turkey.

Corresponding author: Seyfettin Vadi (e-mail: seyfettinvadi@gazi.edu.tr)

This publication has been supported possible with the project numbers 07/2019-16 and 07 / 2020-05 by the Gazi University Sciences Researches Unit.

ABSTRACT This paper proposes a proportional resonant and proportional integral based control strategy for single phase quasi-Z-source inverters (qZSIs) which is able to operate in buck and boost modes. Switching signals of the qZS inverters can be generalized as shoot through and non-shoot through states. The dc-link voltage of the qZSIs can be controlled by generating proper shoot through signals. The control strategy for qZSIs should be able to control both dc and ac-sides at the same time. First, the average state–space model of qZSI is obtained for closed loop control in this paper. Thereafter, the proportional resonant control is designed to achieve ac-side voltage control. Also, voltage control of dc-side capacitor is achieved by using proportional integral control method. Finally, the switching signals are obtained by applying the control outputs to modulation strategy. Experimental results are presented to demonstrate the effectiveness of the control method. The results verify that the proposed control strategy successfully regulates both dc and ac-side control variables.

INDEX TERMS PI controller, PR controller, sinusoidal pulse width modulation, quasi-Z-source inverter.

I. INTRODUCTION

The use of renewable sources is increased due to the lack of fossil fuels and the increasing global energy consumption. Maximum energy harvesting and continuous energy generation from renewable energy sources are essential to meet the increasing demand. The renewable energy applications can be categorized as stand-alone and grid-connected [1-3]. In these applications, power converters are used to convert energy forms. The power converters used for the stand-alone and grid-tied application are divided into several types and configurations [4-6]. One of them is the qZS inverter [7] which is able to operate in buck and boost modes. Maximum energy is produced in these inverters due to the continuous input current feature. Therefore, it is widely preferred in renewable energy applications [8-10].

The qZS inverter is derived from the Z-source inverter topology. ZS inverter is capable to operate in buck and boost modes like qZS inverter. The ZS inverter are commonly used in photovoltaic energy systems. However, the topology isn't enough for constant current operation in photovoltaic system [11]. Therefore, the qZSIs are more preferred due to the following disadvantages of ZS inverters: ZS inverters are insufficient to provide constant current in the photovoltaic system, the source voltage is not wide range, the circuit components are much and the source stress is high. The qZSIs have several advantages such as boost function by the one-stage conversion, continuous input current, reliability and high efficiency due to the shoot-through withstanding capability, low or no in-rush current during start up, low common-mode noise [12,13]. The qZSI is operated the shoot through mode by triggering the lower and upper switches of the phase to obtain the desired DC-link voltage. In the other mode, the qZSI is operated in the non-shoot through mode (inverter mode). The qZS inverter is generated AC output voltage by transform to AC voltage from DC-Link voltage in this mode [14-16]. These operating modes are obtained by using PWM methods.

The PWM methods such as simple boost, constant boost, maxımum boost, space vector are used to generate and control the shoot through states [17]. Simple boost pulse width modulation (PWM) is preferred for low and medium power applications. It has two reference signals, a constant

This work is licensed under a Creative Commons Attribution 4.0 License. For more information, see https://creativecommons.org/licenses/by/4.0/

This article has been accepted for publication in IEEE Access. This is the author's version which has not been fully edited and
content may change prior to final publication. Citation information: DOI 10.1109/ACCESS.2022.3199732

positive and negative signal [18]. It is similar to SPWM and used to Z source inverter.

The qZSIs have attracted considerable attention in power decoupling, photovoltaic/wind power generation, and motor drive in recently years due to the high step-up ratio in a single stage by introducing an impedance network and special modulation strategy. In this paper, a proportional resonant and proportional integral based control strategy for a single qZSI is proposed. In the proposed method, the dc-side capacitor voltage and the ac-side current of the inverter are controlled. 250 W single phase qZSI prototype has been used in the experimental studies to verify the effectiveness of the proposed control scheme.

The rest of the paper is written in the following order: Section II describes the qZSI circuit and operating principles. Section III describes the design and parameters determination of qZSI. Section IV describes design of the dc side and ac side controller for qZSI. Section V describes the experimental results and implementation of a Proportional resonant and proportional integral based control strategy for single phase qZSI and validates the operation of qZSI. Finally, Section VI concludes the paper.

II. QZSI CIRCUIT AND OPERATION

The circuit diagram of the qZSI is depicted in Fig. 1, These inverter is derived from the ZSI topology. The topology, which has high efficiency and reliability, creates the Shoot Through mode by triggering the lower and upper switches of the phase to increase the DC input voltage and obtain the desired output voltage.

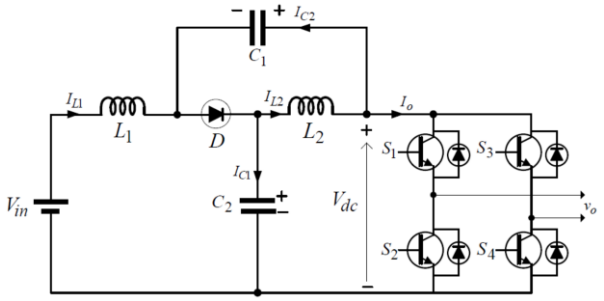

Fig. 1. Circuit diagram of the qZSI Topology

The topology works as an inverter in non-shoot through operation and converts the voltage on the DC link to AC current. The other operation mode is shoot-through mode. In this mode, the topology works as a boost converter. The DC bus voltage is equal to the sum of the energy stored by the C_1 and C_2 capacitors. The total voltage is applied to the inverter as input voltage in non-shoot through mode. In DC side of the inverter, the total voltage or V_{C1} voltage is used as a reference point in a closed loop operation.

Switching signals are required to operate the inverter. These signals are obtained by PWM methods. There are many methods to generate switching signals. One of them is the sinusoidal pulse width modulation (SPWM) method. This method is a widely used in inverters due to its simple structure. This method is shown in Fig. 2. Accordingly, the switching signals are obtained by comparing the sinusoidal signal with carrier signal within the specified range. The difference for this topology from traditional PWM methods is that any arm in the inverter is short-circuited and applied by combining the shoot-through signals created to work as an amplifying circuit with existing sinusoidal PWM signals. PWM signals are obtained as an inverter in the active mode and as a boost converter in the shoot through mode in the method given in Fig. 2. In non-shoot through mode, one and only one device in each phase leg conducts and control of inverter is same as traditional VSI. The shoot through mode occurs when at least one leg is switched on. The voltage across the inverter (V_{PN}) during this mode is zero.

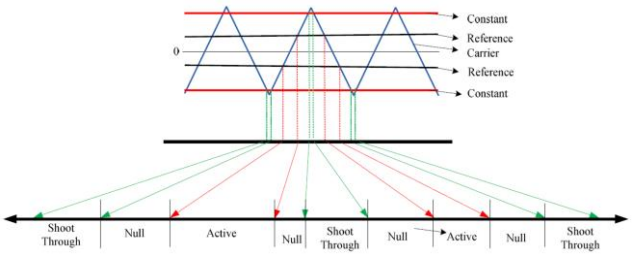

Fig. 2. Control of qZSIs with SPWM (null, active and shoot through states)

The equivalent circuit of the qZSI in case of non-shoot through and shoot through is given in Fig. 3. Mathematical equations were created for both equivalent circuit.

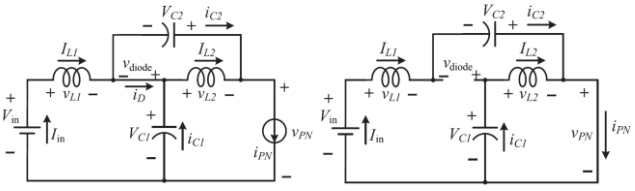

Fig. 3. Equivalent Circuit of qZSI

A. NON SHOOT THROUGH STATE

By considering (Fx = Ax + Bu) state equation, the state-space equations of the qZSI are given in (1)-(3). According to Kirchhoff's Current Law, inductor voltages (V_{L1} and V_{L2}), DC bus voltage (V_{PN}), internal resistances of L and C (R and r) and diode voltage (V_{diode}) are given in (2) and (3).

This work is licensed under a Creative Commons Attribution 4.0 License. For more information, see https://creativecommons.org/licenses/by/4.0/

This article has been accepted for publication in IEEE Access. This is the author's version which has not been fully edited and content may change prior to final publication. Citation information: DOI 10.1109/ACCESS.2022.3199732

$$\begin{bmatrix} L_1 & 0 & 0 & 0 \\ 0 & L_2 & 0 & 0 \\ 0 & 0 & C_1 & 0 \\ 0 & 0 & 0 & C_2 \end{bmatrix} \cdot \begin{bmatrix} \dot{i}_{L1}(t) \\ \dot{i}_{L2}(t) \\ \dot{v}_{C1}(t) \\ \dot{v}_{C2}(t) \end{bmatrix} = \begin{bmatrix} -(R+r) & 0 & -1 & 0 \\ 0 & -(R+r) & 0 & -1 \\ 1 & 0 & 0 & 0 \\ 0 & 1 & 0 & 0 \end{bmatrix} \cdot \begin{bmatrix} i_{L1}(t) \\ i_{L2}(t) \\ v_{C1}(t) \\ v_{C2}(t) \end{bmatrix} + \begin{bmatrix} 1 & R \\ 0 & R \\ 0 & -1 \\ 0 & -1 \end{bmatrix} \cdot \begin{bmatrix} V_{in}(t) \\ I_{PN}(t) \end{bmatrix} \quad (1)$$

$$v_{L1} = V_{in} - V_{C1}, \quad v_{L2} = -V_{C2} \quad (2)$$

$$v_{PN} = V_{C1} - v_{L2} = V_{C1} + V_{C2}, \quad v_{diode} = 0 \quad (3)$$

B. SHOOT THROUGH STATE

In this mode, the state space equations of the inverter model operating as a short circuit are obtained as seen in (4). According to Kirchhoff's Current Law, inductor voltages (V_{L1} and V_{L2}), DC bus voltage (V_{PN}), internal resistances of L and C (R and r) and diode voltage (V_{diode}) are expressed as in (4) and (5).

$$\begin{bmatrix} L_1 & 0 & 0 & 0 \\ 0 & L_2 & 0 & 0 \\ 0 & 0 & C_1 & 0 \\ 0 & 0 & 0 & C_2 \end{bmatrix} \cdot \begin{bmatrix} \dot{i}_{L1}(t) \\ \dot{i}_{L2}(t) \\ \dot{v}_{C1}(t) \\ \dot{v}_{C2}(t) \end{bmatrix} = \begin{bmatrix} -(R+r) & 0 & 0 & 1 \\ 0 & -(R+r) & 1 & 0 \\ 0 & -1 & 0 & 0 \\ -1 & 0 & 0 & 0 \end{bmatrix} \cdot \begin{bmatrix} i_{L1}(t) \\ i_{L2}(t) \\ v_{C1}(t) \\ v_{C2}(t) \end{bmatrix} + \begin{bmatrix} 1 & 0 \\ 0 & 0 \\ 0 & 0 \\ 0 & 0 \end{bmatrix} \cdot \begin{bmatrix} V_{in}(t) \\ I_{PN}(t) \end{bmatrix} \quad (4)$$

$$v_{L1} = V_{C2} + V_{in}, \quad v_{L2} = V_{C1} \quad (5)$$

$$v_{PN} = 0, \quad v_{diyot} = V_{C1} + V_{C2} \quad (6)$$

Equations for the average voltage of capacitors in a steady state switching period are given in (7) and (8).

$$V_{C1} = \frac{T_1}{T_1 - T_0} V_{in} \quad (7)$$

$$V_{C2} = \frac{T_0}{T_1 - T_0} V_{in} \quad (8)$$

Assuming a switching time T, shoot-through operating time T_0, non-shoot-through operating time T_1 and DC input voltage is V_{in}; The DC bus voltage equation of the inverter is obtained as (9). T represents the inverter's switching period ($T_0 + T_1$) and B represents the inverter's boost parameter.

$$v_{PN} = V_{C1} + V_{C2} = \frac{T}{T_1 - T_0} V_{in} = BV_{in} \quad (9)$$

The average current value of L_1 and L_2 inductors are calculated using the system power as seen in (10).

$$I_{L1} = I_{L2} = I_{in} = P/V_{in} \quad (10)$$

Capacitor currents are calculated as in (11) using Kirchhoff's Current Law.

$$i_{c1} = i_{c2} = i_{PN} - I_{L1} \quad (11)$$

The voltage gain (G) of the inverter is calculated using (12).

$$G = \frac{\hat{v}_{in}}{0.5 v_{PN}} = M.B \quad (12)$$

where M is the modulation index, V_{in} is the DC input voltage.

III. DETERMINATION OF qZSI PARAMETERS

For the experiment, V_{in} is chosen as 80 V and d_{st}=0.20 is chosen to yield V_{C1}=120 V based on (12). L and C component values are determined using second harmonic (2ω) suppression formulas (13) and (14). a and b parameters are the current and voltage ripple ratios, respectively. To limit current and voltage ripples, ratios are determined to be as shown in Table 1.

$$L = \frac{aV_{in}(1-d_{sh})}{4\omega bMI_a cos\varphi} \quad (13)$$

$$C = \frac{MI_a(1-2d_{SH})}{a\omega V_{in}}[bcos\varphi + 1] \quad (14)$$

The required capacitance to achieve ε=5% is 1 mF from (14) and a 1.5-mH inductance value will limit the inductor current ripple within 25%. Thus, inductance values (L_1 and L_2) are calculated as 1.5mH and capacitance values (C_1 and C_2) are calculated as 1000 µF according to (13) and (14).

This work is licensed under a Creative Commons Attribution 4.0 License. For more information, see https://creativecommons.org/licenses/by/4.0/

This article has been accepted for publication in IEEE Access. This is the author's version which has not been fully edited and
content may change prior to final publication. Citation information: DOI 10.1109/ACCESS.2022.3199732

TABLE 1. PARAMETERS AND VALUES USED IN EXPERIMENTAL

Definition and Symbols	Value	Definition and Symbols	Value
Input V_{DC} voltage (V_{in})	80 V	Modulation rate (m)	0.7
qZS impedance inductors (L_1-L_2)	1.5mH	Shoot-through duty cycle (d)	0.20
qZS impedance capacitors (C_1-C_2)	1000 µF	Load (R)	20 Ω
LC filter inductor (L_1)	2mH-0,1Ω	Output frequency (f_{out})	50 Hz
LC filter capacitor (C_f)	10 µF	Power (P)	250 W
PI Controller gains (K_p, K_i)	0.2 - 0,0001	AC output voltage (Max)	100 V AC
PR Controller gains (K_p, K_r)	0.002 - 400	Switching method	SPWM
Switching frequency (f_s)	10 kHz	Switch	IGBT

IV. DESIGN OF THE CONTROL STRATEGY

There are two main objectives of the control for the qZSI, which are corresponding to ac and dc side of qZSI. The block diagram of the proposed control strategy is depicted in Fig. 4. Control objectives for qZSI can be defined as regulating dc-link voltage for dc-side and the output voltage for ac-side. It is provided that the difference between the control parameters and the reference value is minimized with the proposed control method.

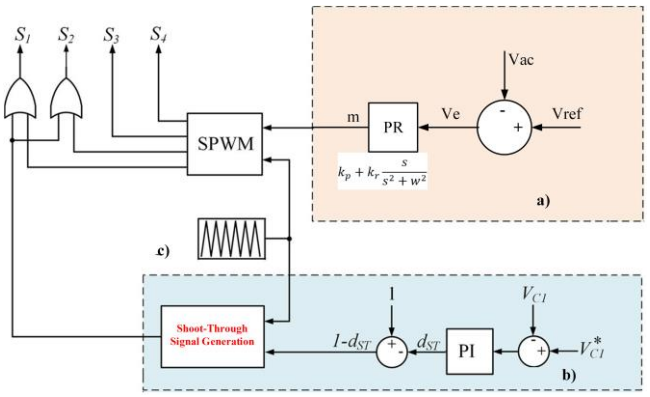

a) AC Side Control b) DC Side Control c) Switching Structure

Fig. 4. Block diagram and switching structure proposed control method

Control of dc and ac side of the qZSI is executed separately, as shown in Fig. 4. Pulses generated by the dc and ac side controller are combined together by logical 'OR'. SPWM method has been used for generating the switching signals. The qZS inverter operates in boost mode owing to the shoot-through signal which is integrated to switching method. The switching signals of the integrated SPWM are given in Fig. 5. While S_1 and S_4 switches work as an inverter, the S_2 switch is activated for a short time and short-circuits the branch where it is located. The input voltage is boosted with the qZS network at the dc side during the shoot-trough time. Simultaneously, while S_2 and S_3 switches work as inverter, the S_1 switch is also activated for a short time and short-circuits the branch where it is located. The input voltage is boosted with the qZS network at the dc side during the shoot-trough time.

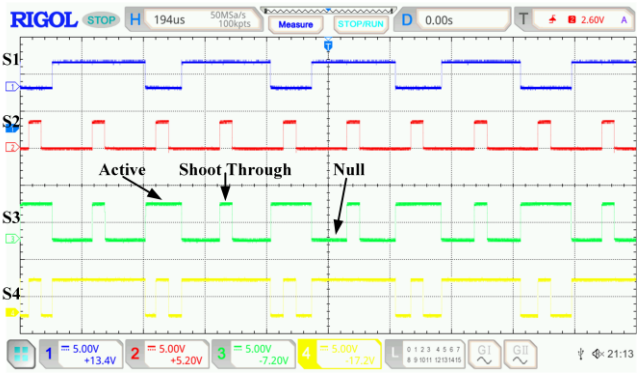

Fig. 5. Switching signals applied to the inverter in experimental

A. DC SIDE CONTROL

The proposed control strategy is structured by considering both dc-side and ac-side of the qZSI. The control method can be defined as regulating the V_{C1} and v_{ac}. The DC side is the impedance circuit of the topology and consists of two inductors, two capacitors and a diode. The control variables on the DC side are I_{L1}, I_{L2}, V_{C1} and V_{C2}. V_{C1} control variable is used commonly in the control of DC side. The DC bus voltage (V_{PN}) is equal to the sum of the capacitor voltages V_{C1} and V_{C2}. For the DC side, one or both of the V_{C1}, I_L or V_{PN} bus voltages are used together to boost the process. Since the pulsating inherent of V_{PN}, the V_{C1} capacitor voltage is preferred as a control parameter for dc-side and the PI control method is applied to dc-side of qZSI. V_{C1}* represents reference value of C_1 capacitor on the impedance circuit. The error signal (e_{VC1}) is obtained by comparing V_{C1} and its reference as follows

$$e_{VC1} = V_{C1}^{*} - V_{C1} \quad (15)$$

The error is applied to a PI controller as follows

$$d_{st} = K_P e_{VC1} + K_i \int e_{VC1} dt \quad (16)$$

where K_p and K_i parameters are the proportional and integral constants, respectively. Clearly, the duty ratio of the shoot-through (d_{st}) signal is obtained. As shown in Fig. 6, the control error in (15) is applied to the PI controller. Finally, the control of dc side is achieved.

This work is licensed under a Creative Commons Attribution 4.0 License. For more information, see https://creativecommons.org/licenses/by/4.0/

This article has been accepted for publication in IEEE Access. This is the author's version which has not been fully edited and
content may change prior to final publication. Citation information: DOI 10.1109/ACCESS.2022.3199732

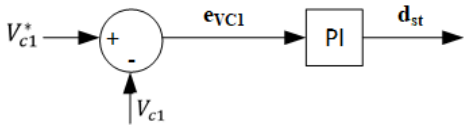

Fig. 6. Block Diagram of 1-dst Equation

B. AC SIDE CONTROL

In the ac side of the qZSI, the control objective is the regulation of the output voltage (v_{ac}). V_{ref} is the reference of v_{ac} which is obtained by multiplying amplitude by a unit sine wave. The voltage error (V_e) is obtained from the difference between the reference voltage and the output voltage as follows.

$$V_e = v_{ref} - v_{ac} \tag{17}$$

The voltage error (V_e) of ac side is applied to a PR controller to achieve the modulation signal. The use of PR controller eliminates the steady state error for ac-side of inverter. Consequently, switching signals are generated by using PI and PR controllers. K_p and K_r parameters in PR controller have been obtained using the trial-and-error method. K_p and K_r parameters are the proportional and resonance constants, respectively.

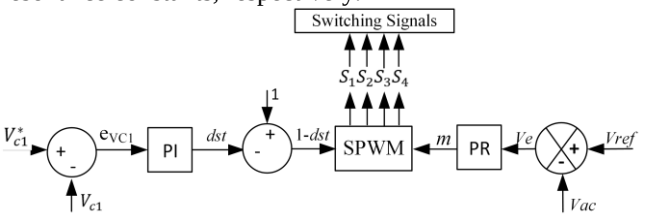

Fig. 7. Closed-loop control block diagram of qZSI

PR controller is defined by only having a high gain in their resonance frequency, allowing it to achieve a zero steady-state error. These controller has a high gain around the resonance frequency. The bandwidth depends on the value of K_r a small value creates a very narrow band, while a large value of K_p cause a larger band around the resonance frequency [22].

C. PARAMETERS DESIGN OF CONTROLLERS

The main control objectives of the qZSI are to regulate dc-side (VC1) and ac-side (vac) variables to their reference values. The PI control method is applied to dc-side of qZSI. The dc-side of qZSI was analyzed with Bode diagram to test stability of PI control method. The Bode plot of the closed-loop PI controller is shown in Fig. 8. When designing the PI parameters, compensating system is determined by the pole-zero locations of the PI regulator with tradeoffs between stability and fast response. It is possible to verify that PI control method with have a similar behavior in the different Kp and Ki values and in the attenuation of low frequency components. However, Case-1 presents a slight superiority in attenuating the components in that range. Regarding the attenuation of high frequency components, the behavior of the three case is different. Case-2 has the worst performance with an attenuation of 45 dB/dec. The Case-1 and Case-3 exhibit an attenuation of 65 dB/dec, although Case-3 presents a slightly superior performance in the attenuation of these components. Regarding the gain margin, Case-3 achieved a higher gain of 12.20 dB, followed by Case-1 with a gain of 7.15 dB, and lastly Case-2 with a gain of 6.35 dB. In terms of phase margin, Case-1,2,3 present a similar value of 130 degrees. The results showed that Case-3 achieved a slightly superior performance than that of Case 1 and 2. Therefore, the PI parameters in Case 3 are used in the implementation.

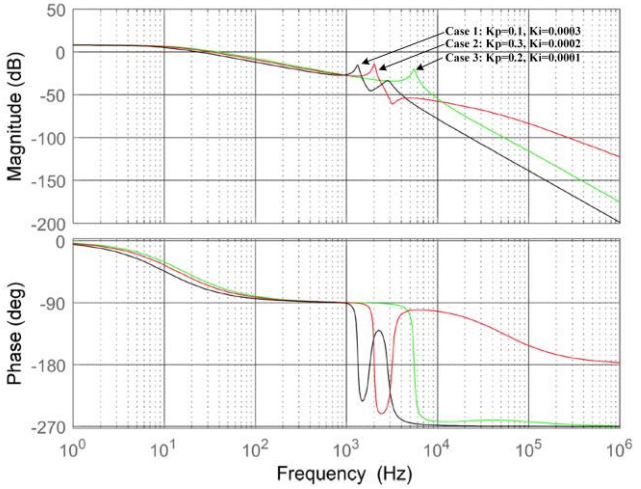

Fig. 8. Bode plots of closed-loop PI controller under various Kp and Ki values. (Kp=0.2 and Ki=0.0001)

The PR controller is used to control the ac-side voltage. The use of PR controller guarantees the zero tracking error of the ac signals in the steady-state [22]. The transfer function of the PR controller can be written as follows

$$G_{PR(s)} = K_p + \frac{2K_r\omega_c s}{s^2+2\omega_c s+\omega^2} \tag{18}$$

where ωc denotes the cut-off frequency, ω denotes the resonant frequency, K_p and K_r denote proportional and resonant gains, respectively. Magnitude and phase responses of the PR controller under various K_p and K_r values are shown in the bode diagram in Fig. 9. The input applied to the PR controller is the output voltage error. Then, the PR controller produces modulation index. The idea behind PR is based on having a sharp peak in the magnitude response of PR controller bode diagram which is located at ω. So, if ω is set to the frequency of v_{ref}, which is 100 π rad/s in this study, then m is generated at the output of PR by controlling v_{ac} such that there is zero steady-state error in the output voltage.

Fig. 9 shows the bode-diagram of the closed-loop transfer functions of the PR voltage controller. The K_P and K_r parameters of the PR controller are determined as K_p=*400* and K_r=*0.002* to provide unit gain (0 dB) and minimum phase error. Thus, these gain values provided accurate control at the resonant frequency. K_p=*400* and K_r=*0.002* values present a slight superiority in attenuating the components in that range. Regarding the attenuation of high frequency components, the behaviour of the three K_P and K_r values are different. K_p=*200* and K_r=*0.001* has the worst performance with an attenuation of 40 dB/dec. The result

This work is licensed under a Creative Commons Attribution 4.0 License. For more information, see https://creativecommons.org/licenses/by/4.0/

This article has been accepted for publication in IEEE Access. This is the author's version which has not been fully edited and
content may change prior to final publication. Citation information: DOI 10.1109/ACCESS.2022.3199732

obtained with $K_p=600$ and $K_r=0.003$ exhibits an attenuation of 60 dB/dec, although $K_p=400$ and $K_r=0.002$ presents a slightly superior performance in the attenuation of these components. Consequently, the PR controller parameters are selected as $K_p=400$ and $K_r=0.002$.

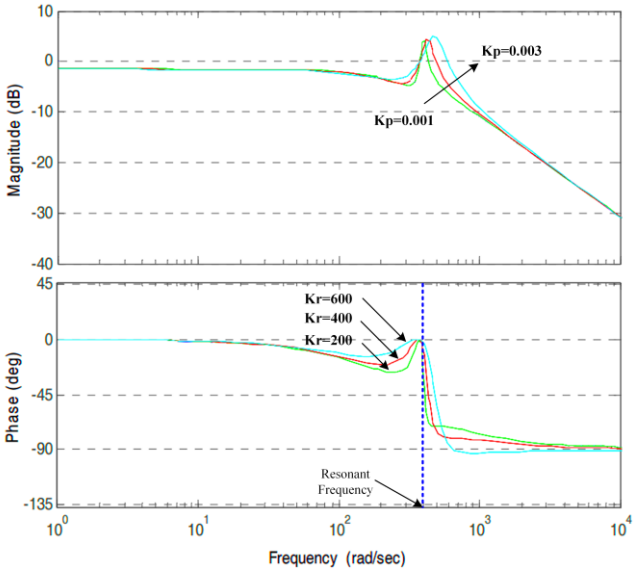

Fig. 9. Magnitude and phase responses of closed-loop PR controller under various Kp and Kr values. (Kp=400 and Kr=0.002)

V. EXPERIMENTAL RESULTS

Experiments have been performed to verify the effectiveness of the proposed control method. To verify the proposed design procedure, a laboratory prototype of the qZS inverter was built. A picture of the prototype of the laboratory prototype is given in Fig. 11. All tests are implemented under the same conditions that are IGBT driver circuit, impedance circuit, current and voltage measurement units, LC filter, main board and load and inverter circuit. Experimental results were obtained from experimental setup the based Texas 28F379D Launchpad. The qZSI prototype is designed with $L_1=L_2=1.5$ mH and $C_1=C_2=1000$ µF using IGBT semiconductor electronic circuit element. The single phase qZS inverter was built with Fuji-2MBI150L-120. A VLA 502-01 hybrid integrated circuit is used to drive the IGBTs. Voltage and current values are measured using Taraz-USM-3IV series isolated voltage and current sensing module. 40 Ω load is connected to the output of the inverter. A programmable voltage source is used as the input source. *LC* filter consisting of 2 mH inductor and 10µF capacitor is connected to the inverter output. The system and control parameters used in the experimental studies are given in Table 1. Steady-state response and dynamic response results are presented to show the performance of the stand-alone operation. The performance and feasibility of the control method is investigated in this section with experimental studies. The block diagram of the complete model is given in Fig. 10.

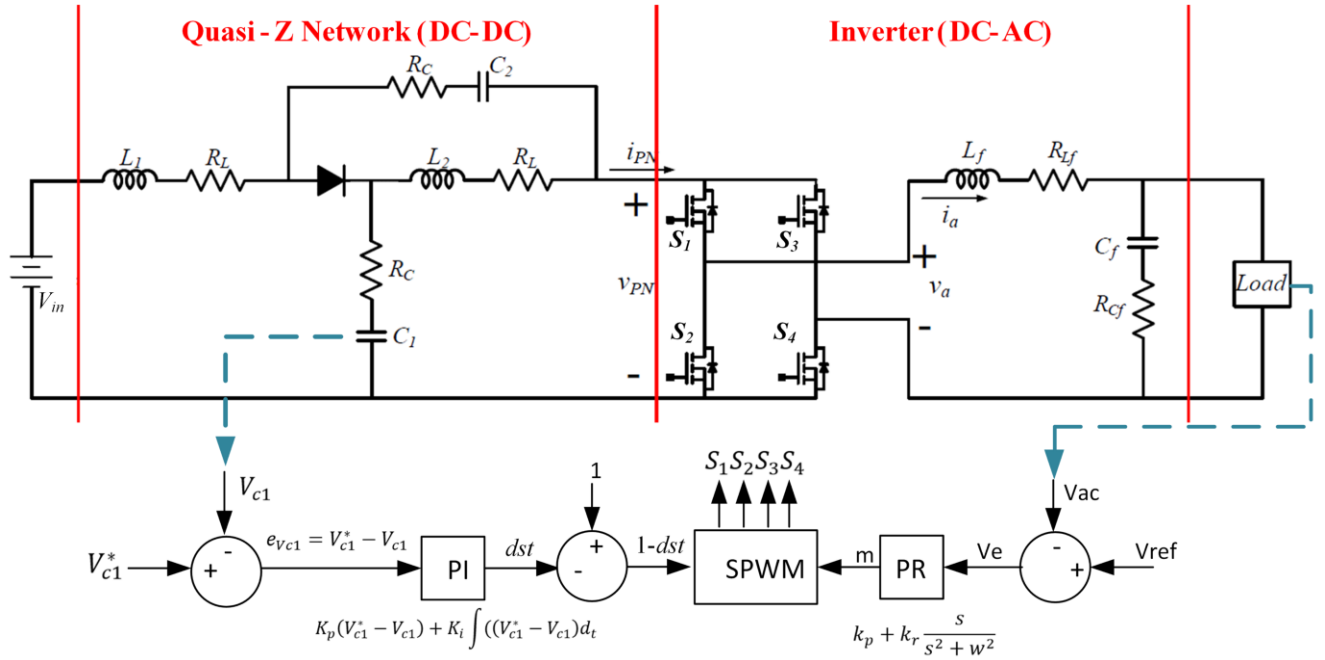

Fig. 10. Block diagram of proposed control method

This work is licensed under a Creative Commons Attribution 4.0 License. For more information, see https://creativecommons.org/licenses/by/4.0/

This article has been accepted for publication in IEEE Access. This is the author's version which has not been fully edited and
content may change prior to final publication. Citation information: DOI 10.1109/ACCESS.2022.3199732

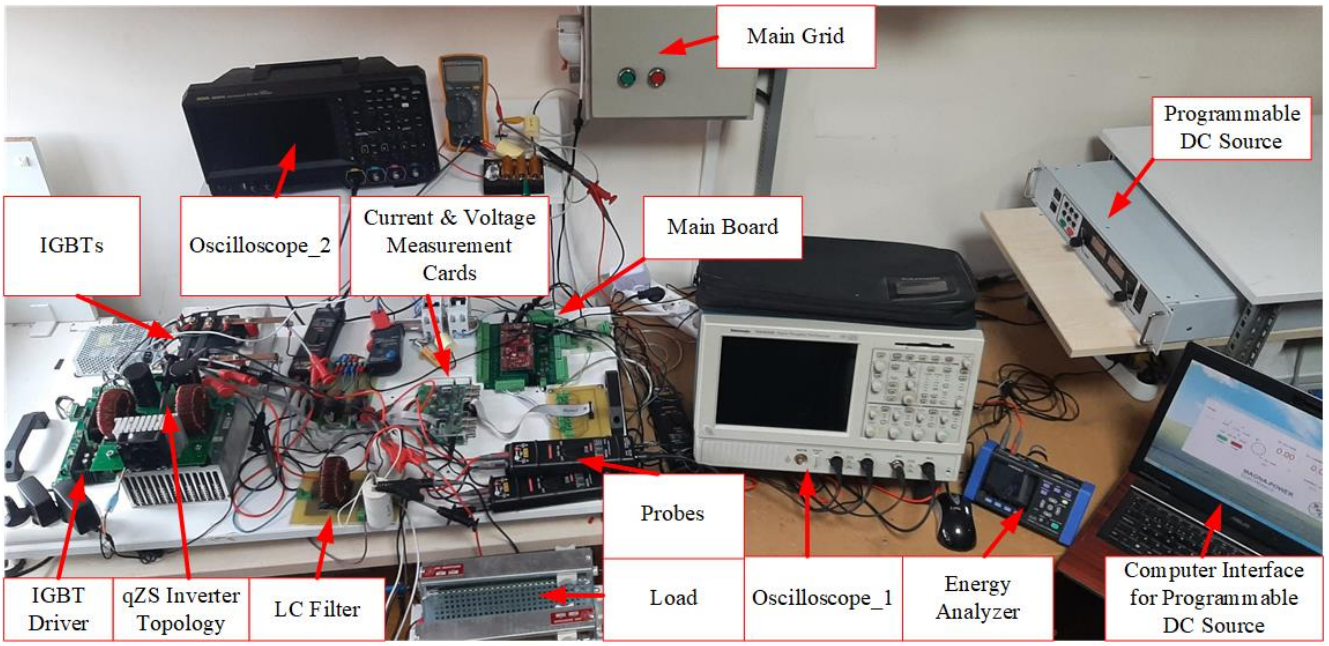

Fig. 11. **Experimental setup**

A - STEADY-STATE RESPONSE RESULTS

Fig. 12 shows the steady-state results of the proposed controller for stand-alone qZSI. The input dc voltage is 80 V, load resistance is 20 Ω, V_{C1}^{*} is 120 V and the reference amplitude of v_{ac} is 100 V in this test. As clearly seen in figure, V_{C1} is regulated to its reference successfully by dc-side controller. Also, the capacitor voltage V_{C2} was measured to be 30 V and DC bus voltage V_{PN} is approximately 150 V. The boost factor and shoot through duty cycle values are approximately 1.875 and 0.233, respectively. The output voltage of the inverter is regulated to 100 V amplitude successfully by PR controller. Both V_{C1} and v_{ac} control parameters ensured stable operation of the qZS inverter according to reference values. This statement is shown in Fig. 12.

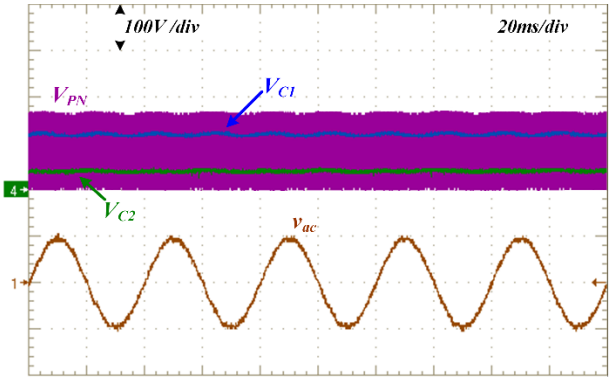

Fig. 12. **Experimental results of steady-state response of DC and AC side variables when V_{in} is 80 V DC, V_{C1^*} is 120 V DC and V_{AC^*} is 100VAC**

The measured total harmonic distortions (THDs) and harmonic components of the load voltage under linear load are shown in Fig. 13. The total harmonic voltage distortion in the output voltage is 1.74%, which is below the recognized standards.

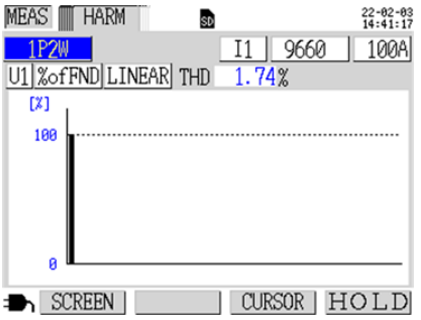

Fig. 13. **THD and harmonic components of the load voltage under a linear load**

B - DYNAMIC RESPONSE RESULTS

To verify the effectiveness of the AC and DC side controllers, dynamic response results for three different scenario are done experimentally.

In the first test, the input voltage and C_1 capacitor reference voltage (V_{C1^*}) are kept as constants at 80 V and 120 V, respectively, while the load value is changed from 40 Ω to 20 Ω. The results obtained under this transition is shown in Fig. 14. When the step change occur the load current in ac side and source current increased from 2.5 A to 5 A, from 1.68 A to 3.33 A, respectively. Although the variations in dc and ac side currents, V_{C1} is regulated to its reference (120V) after the small undershoot.

This work is licensed under a Creative Commons Attribution 4.0 License. For more information, see https://creativecommons.org/licenses/by/4.0/

This article has been accepted for publication in IEEE Access. This is the author's version which has not been fully edited and
content may change prior to final publication. Citation information: DOI 10.1109/ACCESS.2022.3199732

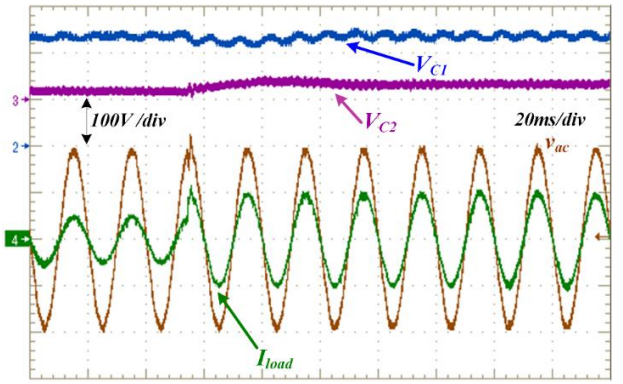

Fig.14 Experimental results of dynamic response of dc and ac side variables when the load changes from 40 Ω to 20 Ω

In the second operation state, it is intended to keep to constant V_{C1} voltage value as 140 V in different input voltages. As shown in Fig. 15, the system initially operates as the input voltage, V_{C1} capacitor voltage, VPN bus voltage and V_{AC} output voltage are 80 V, 120 V, 150 V and 100 V, respectively. During this operation, when the V_{C1} reference voltage is changed from 120 V to 140 V, the V_{PN} bus voltage is measured as 190 V and the V_{AC} output voltage has been kept to constant at 100 V. There is an oscillation in the V_{C1} and V_{C2} capacitor voltage, and V_{PN} bus voltage. But, V_{AC} output voltage is kept constant in reference voltage value thanks to PR controller. The experimental results of the second operation statement are shown in Fig.15.

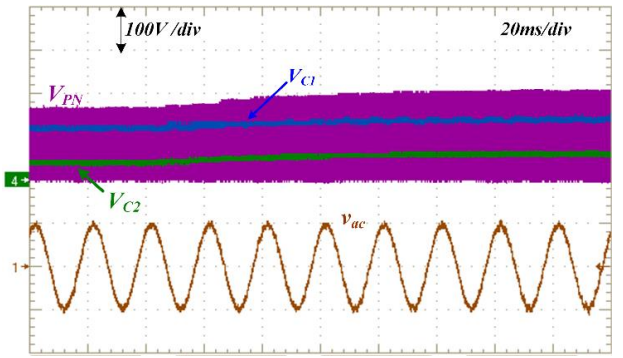

Fig.15 Experimental results of dynamic response of dc and ac side variables when the V_{C1*} changes from 120 V to 140 V under linear load.

In the third operation statement, the C_1 capacitor reference voltage (V_{C1*}) and V_{AC} output voltage are kept as constants at 120 V and 100 V_{AC}, respectively, while the input voltage is changed from 80 V to 100 V. Thus, V_{AC} output voltage operates as stable in the reference output voltage (vo_ref) value for the ac side of qZSI when the V_{in} changes from 80 V to 100 V. When the V_{in} input voltage is changed to 100 V, the V_{C1} capacitor voltage and V_{PN} bus voltage increased from 120 V to 140 V, from 150 V to 170 V, respectively. However, capacitor voltages of V_{C1} and V_{PN} are maintained constant to reference values except the transient period due to the input voltage change. The experimental results of the third operation statement are shown in Fig.16.

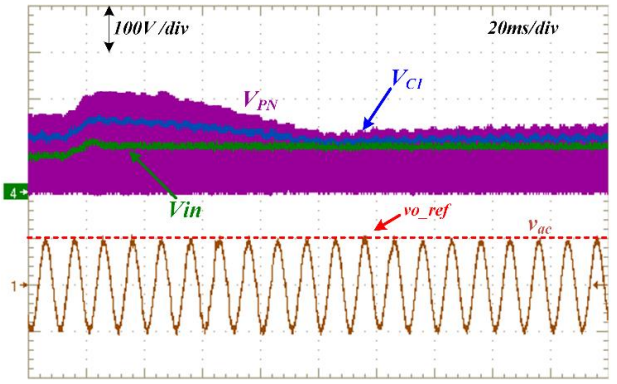

Fig.16 Experimental results of dynamic response of DC and AC side variables when the V_{in} changes from 80 V to 100 V under linear load. Here, "vo_ref" refers to the reference output voltage value for the ac side of qZSI.

In the third operation statement, dynamic response of I_{L1} current is given in Fig.17 while the input voltage is changed from 80 V to 100 V. V_{C1} capacitor voltage and v_{ac} output voltage is kept constant in reference voltage value thanks to PI and PR controller, respectively. I_{L1} current is about 1.2 A. V_{C1} control parameter pass to steady state after the transient time and v_{ac} output voltage is kept constant in reference voltage value thanks to PR controller.

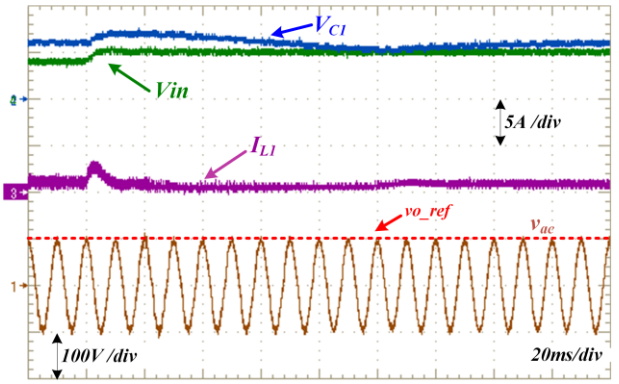

Fig.17 Experimental results of dynamic response of IL1 current when the Vin changes from 80 V to 100 V under linear load. Here, "vo_ref" refers to the reference output voltage value for the ac side of qZSI.

The proposed control method is compared with the existing four control methods introduced in [19] - [22] in Table II. The comparison of these methods with the proposed control method is based on robustness to parameter variations, total harmonic distortion (THD) values of current/voltage, investigation of dynamics response under variations in system variables, number of sensor, sampling frequency and experimental verification. As seen in Table II, the control method in [20] is not robust to parameter variations while the other methods are robust. The dynamic responses of the control methods can be specified as the key performance indicator. The dynamic responses of the proposed method are investigated under variations in all system variables and the satisfactory results are obtained as discussed in the experimental results. Since the effect of the

This work is licensed under a Creative Commons Attribution 4.0 License. For more information, see https://creativecommons.org/licenses/by/4.0/

This article has been accepted for publication in IEEE Access. This is the author's version which has not been fully edited and
content may change prior to final publication. Citation information: DOI 10.1109/ACCESS.2022.3199732

variations in some system variables are not discussed in [20], [21] and [22], the performance of the control methods in these papers are uncertain. The total harmonic distortions can be specified as another important performance indicator. The proposed method offers lower THD than that of [19]-[22], as shown in Table II. The required sensor number is important for simplicity in practical implementation and system cost. The proposed method can be implemented by using only two voltage sensors. Clearly, the required sensor number is less than the methods in [19], [21] and [22], as shown in Table II. Therefore, the proposed method can be implemented easily. Consequently, the proposed method offers advantages in terms of robustness, THD, practical implementation and system cost.

TABLE II. COMPARISON OF FOUR CONTROL METHODS WITH PROPOSED CONTROL METHOD

Description	**[19]**	**[20]**	**[21]**	**[22]**	**Proposed**
Topology	1ϕ qZSI	1ϕ qZSI	1ϕ qZSI	1ϕ qZSI	1ϕ qZSI
Control Approach	DC side: Sliding mode control AC Side : PI control	DC side: Current ripple damping control AC Side : PI control	DC side: Nonlinear control AC side: PR control	DC Side: Model-based current control AC side: PR control	DC side: PI control AC Side : PR control
Robustness to parameter variations	Robust	Robust	Not robust	Robust	Robust
THD of current/voltage	1.96% (THD of current)	Not reported	2.68% (THD of current)	2.6% (THD of current)	1.74% (THD of voltage)
Dynamics response tests under variations in V_{in}, V_{C1}* and *RL*	Variations in V_{in}, V_{C1}* and *RL* are investigated	Not reported	Variations in V_{in} and *RL* are investigated	Variations in V_{C1}* and *RL* are investigated	Variations in V_{in}, V_{C1}* and *RL* are investigated
Number of sensor	3 current 2 voltage	1 current 1 voltage	1 current 2 voltage	2 current 2 voltage	1 current 1 voltage
Sampling frequency	10 kHz	10 kHz	10 kHz	12.5 kHz	10 kHz
Experimental verification	Simulation and Experimental	Simulation and Experimental	Simulation	Experimental	Experimental
On Grid / Standalone	On grid	Standalone	On grid	On grid	Standalone

VI. CONCLUSION

This paper presents a two-stage control method (DC side controller, AC side controller) for qZSI. Controller design for qZSI was carried out a standalone operation. A PR controller was designed for a qZSI. In addition, a classical proportional-integral (PI) controller was designed to regulate the capacitor voltage at its set-point on the dc side. The shoot through control achieves the control of inductor current and capacitor voltage in the qZS network. The steady-state and dynamics response operations of the qZSI are investigated by experimental results. The experimental results verify the effectiveness of the controller. To validate the proposed methodology, steady-state and dynamic responses of dc and ac side variables were considered with different input voltages, reference values and load. Sinusoidal load current with low THD, fast response, as well as robustness under input voltage, reference values and load variations, confirm the effect of the proposed control method. Thus, it is seen that the experimental results for step changes agree with the theoretical results and are proved to be satisfactory.

ACKNOWLEDGMENT

This publication has been supported possible with the project numbers 07/2019-16 and 07/2020-05 by the Gazi University Sciences Researches Unit.

REFERENCES

[1] F. Z. Peng, "Z-Source Inverter," *IEEE Trans. on Ind. Appl.*, vol. 39, no. 2, pp. 504-510, March/April. 2003.
[2] Y. Liu, H. Abu-Rub, and B. Ge, "Z-source/Quasi-Z-source inverters," IEEE Trans. Ind. Mag., pp. 32-44, Dec. 2014.
[3] Y. Li, Joel Anderson, F. Z. Peng and D. Liu. "Quasi-Z Source Inverter for Photovoltaic Power Generation Systems," in *Proc. 2009 IEEE Applied Power Electronics Conf.*, pp. 918-924.
[4] Y. Li, S. Jiang, J. G. Cintron-Rivera, and F. Z. Peng, "Modeling and control of quasi-z-source inverter for distributed generation applications," IEEE Transactions on Industrial Electronics, vol. 60, no. 4, pp. 1532– 1541, 2013.
[5] A. Ayad and R. Kennel, "A comparison of quasi-Z-source inverters and conventional two-stage inverters for PV applications," EPE Journal, vol. 27, no. 2, pp. 43–59, May, 2017.
[6] D. Vinnikov, and I. Roasto, "Quasi-Z-source-based isolated DC/DC converters for distributed power generation," *IEEE Trans. Ind.electron.*, Vol. 58, no. 1, pp. 192-201, Jan. 2011.
[7] W. Liu, Y. Yang, T. Kerekes, E. Liivik and F. Blaabjerg, "Impedance Network Impact on the Controller Design of the QZSI for PV Applications," *IEEE 21st Workshop on Control and Modeling for Power Electronics (COMPEL)*, pp. 1-6, 2020.
[8] L. Monjo and L. Sainz, "State-Space Model of qZSI based PMSG-WPGSs for Transient Dynamic Studies," *IEEE International Conference on*

This work is licensed under a Creative Commons Attribution 4.0 License. For more information, see https://creativecommons.org/licenses/by/4.0/

This article has been accepted for publication in IEEE Access. This is the author's version which has not been fully edited and
content may change prior to final publication. Citation information: DOI 10.1109/ACCESS.2022.3199732

Environment and Electrical Engineering and 2021 IEEE Industrial and Commercial Power Systems Europe (EEEIC / I&CPS Europe), pp. 1-5 2021.
[9] L. Yuan, F.Z. Peng, J.G. Cintron-Rivera, S. Jiang, "Controller design for quasi-Z-source inverter in photovoltaic systems", *Energy Conversion Congress and Exposition (ECCE)*, 2010 IEEE, pp: 3187 – 3194.
[10] L. Yushan., H. Abu-Rub., G. Baoming. "Z-source/quasi-Z-source inverters: derived networks, modulations, controls, and emerging applications to photovoltaic conversion",*IEEE Industrial Electronics Magazine*, Vol. 8, No. 4. pp. 32-44, Dec. 2014.
[11] M. Shahparasti, A. S. Larijani, A. Fatemi, A. Y. Varjani, M. Mohammadian, "Quasi Z-source Inverter for Photovoltaic System Connected to Single Phase AC Grid" Power Electronic & Drive Systems & Technologies Conference2010, pp. 456-460.
[12] A. V. Sieber, H. Haimovich, M. E. Romero, "Control-oriented Modelling and Adaptive Control of a Single-phase Quasi-ZSource Inverter," IECON 2013 - 39th Annual Conference of the IEEE Industrial Electronics Society, pp. 572-577, 2013.
[13] D. Sun, B. Ge, X. Yan, H. Abu-Rub, D. Bi, F. Z. Peng "Impedance design of quasi-Z source network to limit double fundamental frequency voltage and current ripples in single-phase quasi-Z source inverter," 2013 IEEE Energy Conversion Congress and Exposition, pp. 2745 – 2750, 2013.
[14] D. Sun, Dongsen, B. Ge, H. Zhang, X. Yan, D. Bi, H. Abu- Rub, and F. Z. Peng. "An Energy Stored Quasi-Z Source Cascaded Multilevel Inverter Based Photovoltaic Power Generation System." In Applied Power Electronics Conference and Exposition (APEC), 2014 Twenty-Ninth Annual IEEE, pp. 1747-1751. IEEE, 2014.
[15] E. P. P. Soares-Ramos, L. de Oliveira-Assis, R. Sarrias-Mena, P. García-Triviño, C. A. García-Vázquez and L. M. Fernández-Ramírez, "Large-Scale Wind Turbine With Quasi-Z-Source Inverter and Battery," *22nd IEEE International Conference on Industrial Technology (ICIT)*, pp. 403-408, 2021.
[16] A. Abdelhakim, F. Blaabjerg, and P. Mattavelli, "Modulation schemes of the three-phase impedance source inverters – part i: Classification and review," IEEE Trans. on Ind. Electron., vol. 65, no. 8, pp. 6309–6320, Aug 2018.
[17] T. Kayiranga, H. Li, X. Lin, Y. Shi, and H. Li, "Abnormal operation state analysis and control of asymmetric impedance network-based quasi-z source PV inverter" IEEE Trans. on Power Electron., vol. 31, no. 11, pp. 7642–7650, Nov 2016.
[18] R. Dogga and M. K. Pathak, ''Recent trends in solar PV inverter topologies,'' Sol. Energy, vol. 183, pp. 57–73, May 2019.
[19] U. K. Shinde, S. G. Kadwane, S. P. Gawande, M. J. B. Reddy and D. K. Mohanta, "Sliding Mode Control of Single-Phase Grid-Connected Quasi-Z-Source Inverter," in IEEE Access, vol. 5, pp. 10232-10240, 2017.
[20] B. Ge et al., "Current Ripple Damping Control to Minimize Impedance Network for Single-Phase Quasi-Z Source Inverter System," in IEEE Transactions on Industrial Informatics, vol. 12, no. 3, pp. 1043-1054, June 2016.
[21] F. Fang, Y. Li, R. Zhang and Y. Liu, "An nonlinear control strategy for single-phase Quasi-Z-source grid-connected inverter," IECON 2017 - 43rd Annual Conference of the IEEE Industrial Electronics Society, 2017, pp. 7685-7690.
[22] H. Komurcugil, S. Bayhan, F. Bagheri, O. Kukrer and H. Abu-Rub, "Model-Based Current Control for Single-Phase Grid-Tied Quasi-Z-Source Inverters With Virtual Time Constant," in IEEE Transactions on Industrial Electronics, vol. 65, no. 10, pp. 8277-8286, Oct. 2018.



SEYFETTIN VADI (Student Member, IEEE) received the master's degree from the Gazi University Institute of Science, in 2013, where he is currently pursuing the Ph.D. degree. He is also working as a Lecturer with the Department of Electronics and Automation, Vocational School of Technical Science, Gazi University, Ankara. He has published articles are scanned by SCI, SCI-EXP, SSCI, AHCI, and other noteworthy indices. His areas of interest include automation systems, SCADA systems, energy monitoring and control systems, reactive power compensation, software development, microcontrollers, and power electronics.



Prof. Dr. Ramazan BAYINDIR, completed his undergraduate studies at Gazi University, Electrical Education Dep. in 1992 and received his M.Sc. and Ph.D. degrees from the Institute of Science & Technology, Gazi University in 1998 and in 2002 respectively.
Dr. Ramazan BAYINDIR worked as a Research Assistant, Assistance Professor in Electrical Education Department at Gazi University. He became an Assoc. Prof. at Electrical & Electronics Engineering Dep. at Gazi University. Currently, he is working as a Professor at the same department. His main expertise field include renewable energy sources, microgrids, distributed generation, smart grid applications and industrial automation with programmable logic controller (PLC). He has been a program chair to the annual conference of "International Conference on Renewable Energy Research and Applications (ICRERA 2012-2021)", International Conference on Smart Grid (icSmartGrid 2012-2021), 16th International Power Electronics and Motion Control Conference and Exposition (PEMC 2014) and International Conference on Power Engineering, Energy and Electrical Drives, (POWERENG 2013) conference. He served as guest editors for same SCI-indexed reputable journals. He also served as reviewer to many high ranked scientific journals. Dr. Bayindir is currently a Member of the Editorial Board of Tübitak Turkish Journal of Electrical Engineering & Computer Sciences and Editor of IEEE Access.
Dr. Bayındır has more than 250 journal papers and conference papers within his field of work. He has also published as an author in 4 national books and 2 international books. Having completed many national projects, Dr. Bayındır also took part in the project in which many European countries are participants.
He has some key qualifications such as education and curriculum design and development on different fields, vocational and technical education, designing, organization and planning the international level projects, educational and vocational training material development. He is Senior Member IEEE, also PEMC Executive Committee Member.
Dr. Bayındır served as the Vice Dean of the Faculty of Technology, the Director of the Gazi Vocational School, the Faculty of Technology, the Head of the Electrical and Electronics Engineering Department in academic units. He is currently the Vice Rector of Gazi University.

This work is licensed under a Creative Commons Attribution 4.0 License. For more information, see https://creativecommons.org/licenses/by/4.0/